

NUMERICAL SIMULATION AND EXPERIMENTAL STUDY ON SEMI-SOLID FORMING PROCESS OF 319S ALUMINUM ALLOY TEST BAR

Zihan Lang, Feng Wang , Zhi Wang, Le Zhou, Pingli Mao and Zheng Liu

School of Materials Science and Engineering, Shenyang University of Technology, Shenyang 110870, Liaoning, People's Republic of China

Key Laboratory of Magnesium Alloys and the Processing Technology of Liaoning Province, Shenyang 110870, People's Republic of China

Wei Wang

Key Laboratory of Magnesium Alloys and the Processing Technology of Liaoning Province, Shenyang 110870, People's Republic of China

School of Science, Shenyang University of Technology, Shenyang 110870, China

Copyright © 2022 American Foundry Society
<https://doi.org/10.1007/s40962-022-00788-8>

Abstract

The semi-solid high-pressure die casting is playing an increasingly important role in the field of automotive lightweight. Herein, a numerical simulation study on the semi-solid die casting process of 319s aluminum alloy test bars was carried out. By setting different die casting process parameters for simulation calculation, the defect location, distribution, and content were analyzed in this paper. The best die casting process parameters were determined, which were with injection rate of 1 m/s and die casting temperature of 570 °C. According to the simulated defect location, the overflow system of the test bar was optimized, including the design of the overflow groove, sprue and venting channel. The semi-solid slurry was prepared by the Swirled Enthalpy Equilibration Device. Trial production of the test bar was carried out with the

best die casting process parameters. The casting product is well filled and has no obvious defects. The experimental results show that the microstructure of test bar has fine and rounded grains with an average size of 28.27 μm and an average shape factor of 0.86. After T6 heat treatment, the transformation of the morphology and distribution of the strengthening phases plays a crucial role in the improvement of mechanical properties. The tensile strength increases from 269 MPa of 319s-F to 395 MPa of 319s-T6, but the elongation decreased slightly from 7.3 to 6.2 %.

Keywords: semi-solid die casting, numerical simulation, process parameters, microstructure, mechanical properties

Introduction

High-pressure die casting (HPDC) of Al–Si alloy is a low-cost process for the production of castings in large quantities and with high dimensional accuracy. However, due to the turbulent flow of liquid metal in the mold cavity, it is easy to form the defects of entrainment air and oxide inclusions in the process of HPDC, which will reduce the quality of the castings.¹ The viscosity of semi-solid metal is

higher than that of liquid metal, and the filling speed of slurry is low during semi-solid die casting, so it can prevent the turbulence of slurry in the filling process and reduce the possibility of air entrainment, which will eliminate the disadvantage of HPDC.²

The semi-solid forming process can obviously improve the casting quality and mechanical properties, which is a near-net-shape technology that shapes castings in a semi-solid state in the temperature range between the solidus and the liquidus. It is expected to play a greater role in the field of automotive lightweight in the future.^{3,4} At present, semi-solid metal processing application is the most successful

and most widely used in the preparation of aluminum alloy. It is not only because of the low melting point and wide application range of aluminum alloy, but also because of the wide liquid–solid coexistence zone of aluminum alloy system.⁵ The alloy state of semi-solid die casting is different from that of liquid die casting, as well as the main die casting parameters and the design of the casting system are also obviously different.⁶ At present, there is much research on the liquid die casting at home and abroad, but there is little related research on the semi-solid. Nourouzi et al.⁷ investigated the optimal forming process parameters of semi-solid slurry prepared by cooling slope method for A356 alloy and obtained the smallest grain structure by optimizing three process parameters, including refrigeration coefficient, pouring temperature and die cavity temperature. Dumani et al.⁸ studied the effects on casting time, shrinkage rate and bubble formation in semi-solid high-pressure die casting process of three technological parameters, including liquid phase fraction of slurry, second phase plunger velocity and mold geometry.

With the development of die casting products toward diversification and complexity, various casting defects will inevitably occur in the actual die casting production. According to the traditional methods in the past, the molds are constantly adjusted and tested based on the quality of the castings. It is not enough to guarantee the quality of casting products purely based on experience. However, the die casting process and the casting system can be analyzed and inspected by numerical simulation, which displays the possible defects of the casting under the corresponding die casting process parameters and the location of the defects.^{9,10} By using numerical simulation to analyze the casting process, the filling and solidification process can be reproduced more truly, and the distribution of flow field, temperature field and stress field in the casting process can be deeply analyzed. Product defects can be predicted and better solutions can be found by using simulation methods. Based on above methods, the process design and mold structure are optimized, the quality of parts is improved, the trial production cycle of products is shortened, production costs are reduced, as well as the economic benefits of casting production and product competitiveness are improved.^{10,11} Ren Shuyang et al.¹² designed the pouring system of aluminum alloy semi-solid die casting by numerical simulation and determined the best casting temperature, injection speed, and mold temperature. Bhunia et al.¹³ studied the temperature, viscosity, speed and pressure in the filling process of A356 aluminum alloy through numerical simulation and determined the optimal technological parameters. And the microstructure and properties of semi-solid die-cast aluminum alloy steering knuckle were also discussed in their paper. C.G. Ang et al.¹⁴ used Magmasoft software to conduct numerical simulation and shrinkage cavity prediction on the forming process of semi-solid die casting under different injection rates and obtained the optimal injection rate and structural

parameters of mold design. M. Perez et al.¹⁵ used the lattice model concept to conduct numerical simulation of the separation and polymerization process of semi-solid slurry under shear force and revealed the variation law of slurry viscosity with shear rate and solid rate, as well as the nucleation law and structural morphology of three-dimensional radicals under shear stress.

In summary, numerical simulation of casting process provides a new research idea for casting process, and its importance is widely recognized, so Flow-3D simulation software is used to simulate and analyze the die casting process of aluminum alloy test bars in this paper. The casting structure and process parameters were optimized and improved through the analysis of the die casting defects of the castings. According to the best process parameters, the test bar was trial-produced, and the mechanical properties and product quality of the test bars were advanced.

Numerical Simulation and Experimental Method of Semi-solid Die Casting

Establishment of test bar model and parameter selection

Flow-3D is a three-dimensional computational fluid dynamics and heat transfer analysis software developed by FLOW Science in the USA. Its functions include importing problem solving space, meshing, defining boundary conditions, simulation solving, rendering of simulation results, etc. It is easy to use, with strong engineering applicability. Since the commercial version was officially launched in 1985, it has been widely used in the field of fluid dynamics simulation.¹⁶

The VOF (Volume of Fluid) model¹⁷ is one of the core technologies of Flow-3D. It is a method used to simulate the complex flow of computational fluid free surface. This unique method is the most advanced method for tracking the free liquid level, which can trace the free liquid level by solving a set of continuity equation and momentum equation. Another core technology, FAVOR (Fractional Area/Volume Obstacle Representation) technology,^{18–20} is the flexible combination of the advantages of the rectangular grid with the twisted and adaptive grid. This technique, which simulates complex shapes based on the percentage of area and volume, is one of the key features of this software. It is used in the finite-difference rectangular grids to prevent zigzag boundaries.

Figure 1 is a schematic diagram of the simulation process of the software. The simulation process is shown as follows: Firstly, a three-dimensional model was imported and a physical model and fluid material were selected, as well as a virtual mold was established. Then, the finite

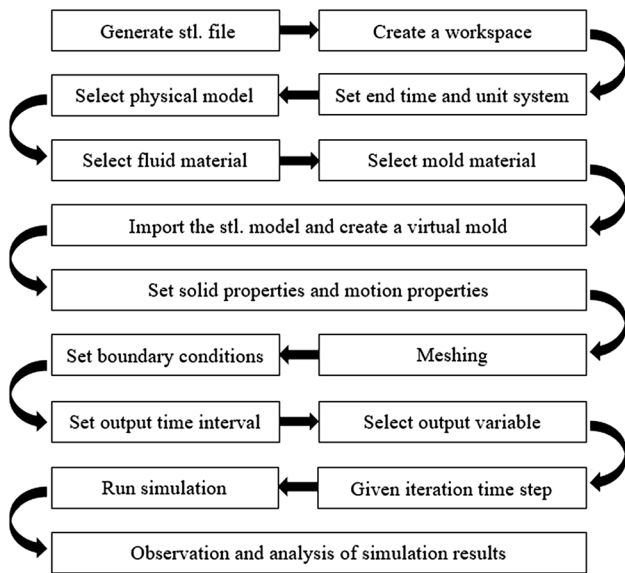


Figure 1. Schematic diagram of the simulation process.

difference method was used to divide the grid, which was structured hexahedral. This software can use the method of multi-grid and block combination to divide different areas of the model to avoid the waste of the grid and reduce the simulation time and difficulty. Thirdly, the boundary conditions and the simulation parameters were set, which were the prerequisites for the governing equation to have a definite solution. Generally speaking, initial conditions can affect the convergence speed of the results, while the boundary conditions can control the flow form. Therefore, to obtain more accurate simulation results, it is particularly important to select appropriate boundary conditions and initial conditions. The setting of simulation parameters includes 319s aluminum alloy, whose chemical composition (Table 1) and thermophysical properties (Table 2) are obtained from the software database. The basic parameter settings of the numerical simulation process are shown in Table 3. Finally, the simulation calculation and result analysis were carried out. The establishment of a 3D model of the test bar completed by the drawing software UG is shown in Figure 2.

Viscosity factor is the key basis and important parameter of semi-solid numerical simulation, which is different from that of conventional die casting simulation. Through experiment and software calculation, the data of viscosity change of 319s aluminum alloy with temperature was measured, and Origin was used to draw the corresponding

Table 1. Chemical Composition of 319s Aluminum Alloy

Alloy	Si	Cu	Mg	Fe	Ti	Sr	Al
wt%	6.0	3.0	0.33	0.12	0.2	0.04	Bal.

Table 2. Thermal Physical Properties of 319s Aluminum Alloy

Solidus/°C	Liquidus/°C	Latent heat of fusion/(kJ·kg ⁻¹)
508	612	400

Table 3. Die Casting Simulation Parameter Setting

Simulation parameters	Values
Initial mold temperature/°C	280
Die casting temperatures/°C	580, 590, 600
Injection velocities/(m·s ⁻¹)	0.5, 1, 1.5, 2
Mold material	Steel H-13
Heat transfer coefficient between mold and mold(W/m ² K)	1000
Heat transfer coefficient between material and mold(W/m ² K)	2700
Size of cells	0.01

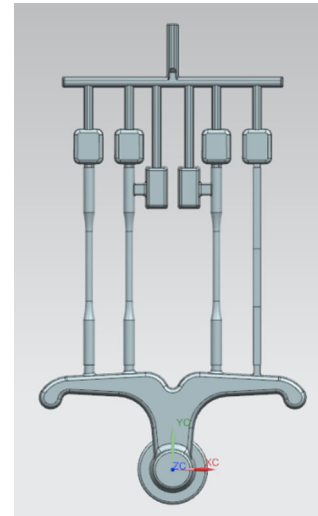


Figure 2. Test bar model.

curve, as shown in Figure 3. The data of solid-phase fraction change of 319s aluminum alloy with temperature were obtained by Jmatpro, and its curve is shown in Figure 4. Meanwhile, the solidus and liquidus temperatures were measured to be 508 °C and 612 °C, respectively.

The equivalent viscosity of the solid–liquid coexistence zone can be calculated by the “Mori– Etsuke” empirical formula as follows:

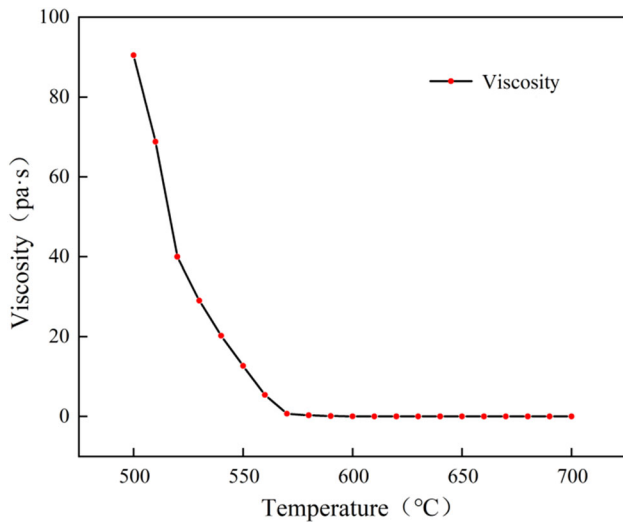


Figure 3. Curve of 319s aluminum alloy viscosity vs. temperature.

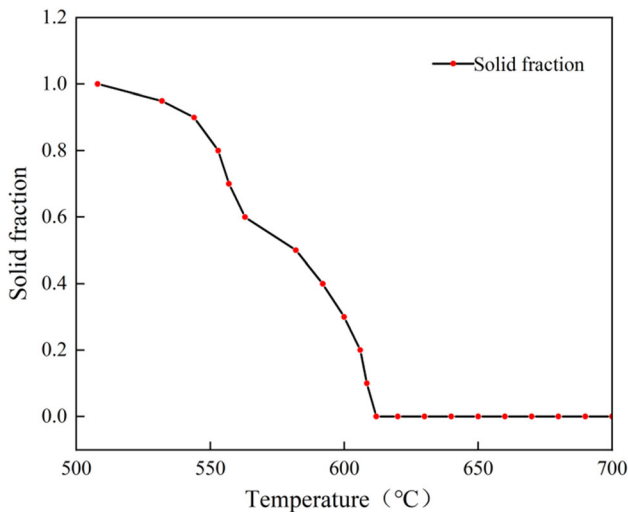


Figure 4. The solid fraction of 319s aluminum alloy vs. temperature.

$$\mu = \mu_0 \cdot \{1 + k/(1/fs - 1/fsc)\} \quad \text{Eqn. 1}$$

where μ is the equivalent viscosity of the solid-liquid coexistence zone, μ_0 is the viscosity of the pure liquid-phase metal, k is the shape coefficient of the solid particles, fs is the solid-phase ratio, fsc is the flow stop critical solid rate in mori-Etsuke empirical formula. Among them, the shape coefficient k represents the influence coefficient of solid particles on the equivalent viscosity, which can be solved by the following calculation formula:

$$K = D \cdot S/2 \quad \text{Eqn. 2}$$

where D is average diameter of solid-phase particles, S is

specific surface area (surface area/volume) of solid-phase particles.

Structural design optimization of test bar casting system

During the semi-solid die casting process of aluminum alloy, entrainment air defects are easily generated at the junction of slurry, the edge of cavity and the final filling of slurry. Therefore, it is necessary to carry out a series of filling simulation experiments to analyze the defects position before die casting and optimize the corresponding structural design of the model according to the generated defects. In order to reduce the defects caused by the internal filling of the casting and improve the casting performance and quality, it is necessary to install an overflow system on the casting. The setting of the overflow grooves can play the role of collecting air and oxidized inclusions. The exhaust duct can effectively exhaust the trapped air inside the casting.

Preparation method of semi-solid slurry and die casting of test bar

The 319s aluminum alloy was put into a pit-type crucible resistance furnace for melting. The heating temperature was set at 700 °C. After the metal was completely melted, the temperature was adjusted to 720 °C for heat preservation. In the process of melting, the alloy is easy to react with oxygen in the air due to the high temperature, which leads to the existence of oxidized inclusions and gases in the melt. This results in casting defects such as shrinkage cavities, shrinkage porosity, and cracks, which seriously affect the mechanical properties and products of the castings quality.²¹ Therefore, the metal molten liquid needs to be refined and degassed. The pulse rotary injection process was used in this experiment.²² After degassing, the molten metal was stood for 20 minutes and then carried out deslagging. The formation of oxide inclusion defects is that during the solidification process of liquid aluminum, with the decrease in temperature, the solubility of oxygen in liquid aluminum drops, and oxygen reacts with other elements in liquid aluminum to form oxides; or in the pouring process, the liquid aluminum with not effective protection, will occur secondary oxidation with the surrounding environment and then oxide will be generated. At present, X-ray scanning, industrial CT and ultrasonic detection methods are used to detect oxides. The most widely used method is X-ray scanning, whose basic principle is based on the weakening and absorption characteristics of radiation in the detected object, which is related to the absorption capacity radiation and properties of materials.

Semi-solid slurry was prepared by SEED method.^{23,24} The process flow is shown in Figure 5. The crucible rotation

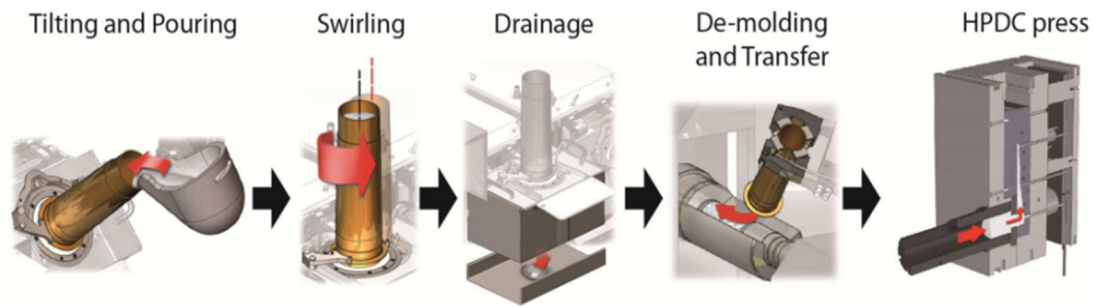


Figure 5. Schematic diagram of SEED slurry preparation process.

time and rotation rate were strictly controlled, and the temperature change of molten liquid was monitored by infrared electronic thermometer in the preparation process. The specific pulping process parameters are as follows: molten metal pouring temperature of 650 °C, crucible rotation frequency of 40 Hz, rotation time of 75 s.

Results and Discussion

Analysis of Simulation Results of Test Bar

The Effect of Injection Rate on Semi-Solid Die Castings

In the semi-solid die casting process of aluminum alloy, numerical simulation was carried out by setting different filling speed. And the best injection rate was determined by analyzing the results and observing the occurrence of casting defects. Due to the small size of the inner gate, the filling speed of the metal slurry is accelerated after passing through the inner gate. In order to ensure that the slurry is accumulated at the inner gate first and can fill the cavity smoothly from bottom to top, a lower injection rate is needed for die casting, which is conducive to the discharge of gas and greatly reduces the potential for gas entrapment. The specific process parameters are die casting temperature of 580 °C and mold temperature of 260 °C. Simulation was carried out with four speed modes of 0.5, 1.0, 1.5 and 2.0 m/s, respectively. The simulated visual presentation of the volumetric distribution of entrained air defects and the mass volume of oxide inclusion defects as a function of injections speeds are displayed in Figure 6. This is then shown graphically for the various injection velocities as entrained air volume vs. filling time in Figure 7(a) and mass volume of oxide inclusion defect vs. filling time in Figure 7(b).

It can be seen from Figures 6 and 7 that as the injection rate increases, the entrainment content of the casting increases gradually. This is because too fast filling speed will lead to more intense collision between molten metal and cavity wall, causing the molten metal to flow by high-velocity in front of the air. Besides, the speed of backflow is fast and

the air has no time to remove, which will cause the phenomenon of entrainment air. At the same time, the injection speed is also too fast and the filling time is short, which is not conducive to the discharge of gas. Judging from the distribution of entrainment air in Figure 6, except for the overflow groove at the top, most entrainment air defects exist at the top of the two middle test bars. It can be seen that when the injection rate is 0.5 m/s and 1 m/s, entrainment air defects at the top of the test bar are less distributed, and entrainment air defects are the most serious when the injection rate is 2 m/s. It can be clearly seen from the curve of the entrainment air content as the time measured that the increase rate of entrainment air content is obviously accelerated at two specific time nodes. Taking the simulation with a speed of 1 m/s as an example, according to the filling simulation animation, find the corresponding time node for observation and analysis, as shown in Figure 8. It can be seen that the sudden increase in entrainment air content between node 1 and node 2 is caused by the severe entrainment air generated at the upper end of the test bar, while the substantial increase in entrainment from node 2 to node 3 is due to the severe entrainment inside the overflow groove. Therefore, it is more accurate to show the influence of injection velocity on the quality of the test bar by using the gas content between node 1 and node 2. At the rate of 0.5 m/s, the gas content of the test bar is at least about $1.91 \times 10^{-6} \text{ m}^3$, followed by $2.35 \times 10^{-6} \text{ m}^3$ at the rate of 1 m/s.

The oxidized slag content of the casting gradually decreases with the increase in the injection rate. This is because with fast flow rate and short filling time, the time for the metal to react with oxygen when filling the mold is reduced. The distribution of oxide inclusions in Figure 6 and the fitting curve in Figure 7 show that when the injection rate is 0.5 m/s, the internal oxide inclusion defects in the casting are very serious, and the content is significantly higher than those at other injection rates. There is no significant difference in the content of oxide inclusions in the other three rates. Therefore, the injection rate of 1m/s is the most suitable for semi-solid die casting of the test bar.

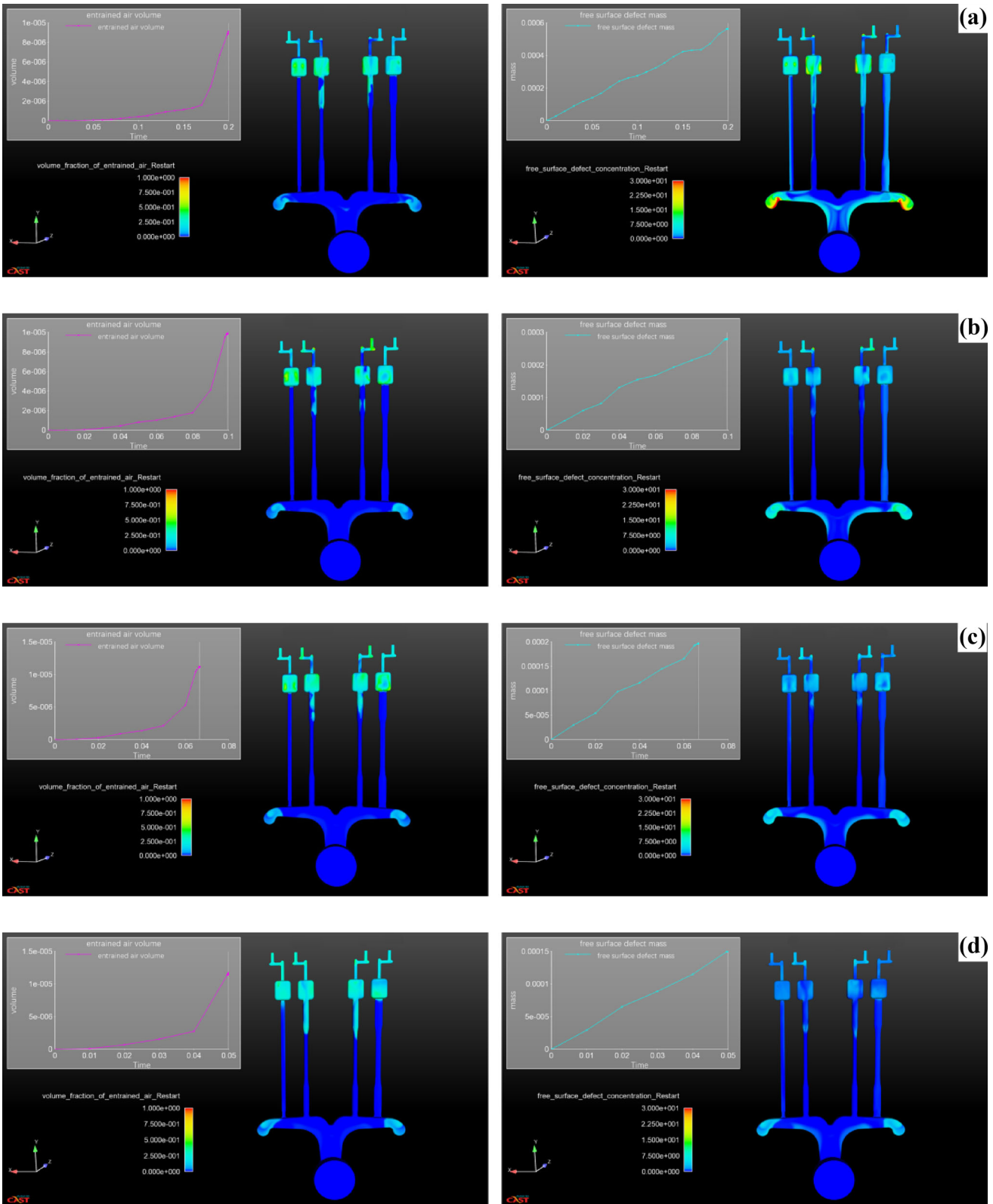


Figure 6. Defect distribution of entrainment air and oxide inclusions at different injection rates (a) 0.5 m/s, (b) 1 m/s, (c) 1.5 m/s, and (d) 2 m/s.

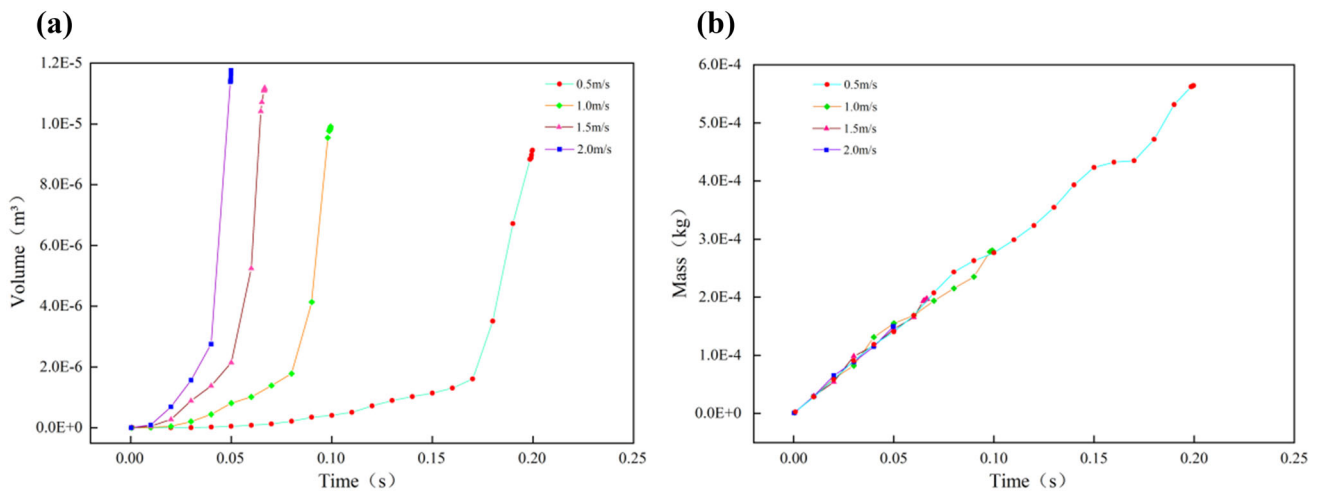


Figure 7. Defect contents vs. filling time at different injection rates (a) entrainment air, (b) oxide inclusions.

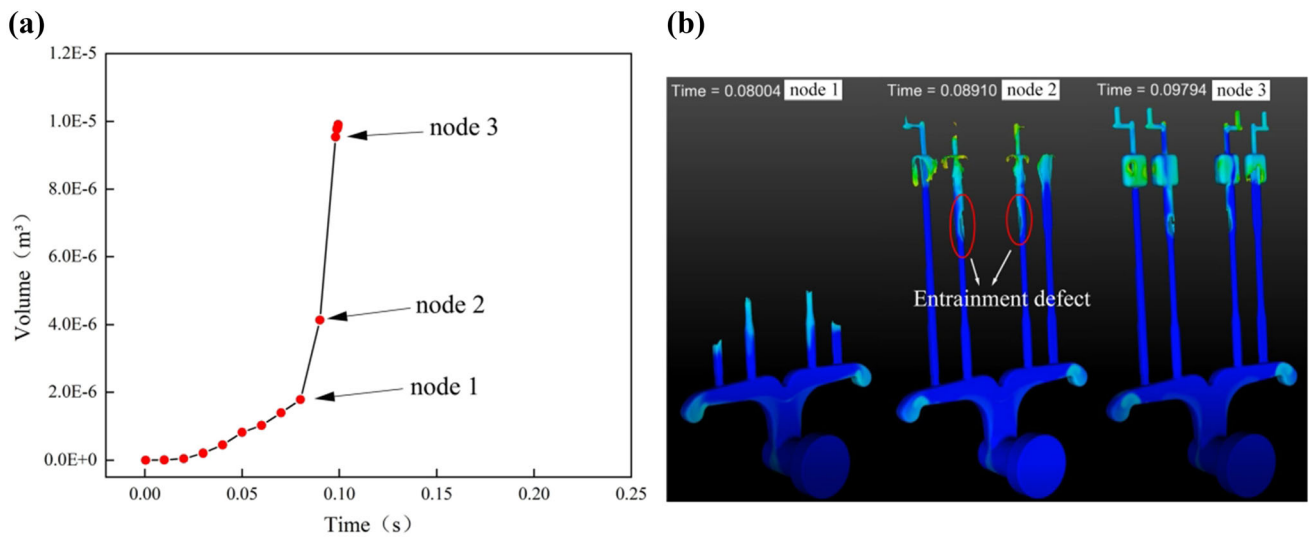


Figure 8. Entrainment air content corresponding to each time node at 1m/s injection rate.

The Effect of Die Casting Temperature on Semi-Solid Die Castings

die casting temperature is also an important factor that affects the forming quality of semi-solid die castings. Simulation is performed by setting different die casting temperature process parameters to observe the occurrence of casting defects, so that the best die casting temperature can be determined. The semi-solid die casting effect is best when the solid-phase fraction of the metal slurry is between 0.3 and 0.7. Higher solid fraction can make the molten metal fill smoothly and reduce the generation of oxidation inclusions and pore shrinkage.²⁵ Therefore, three die casting temperatures of 570, 580, and 590 °C were used for numerical simulation (injection rate of 1.5 m/s, mold temperature of 260 °C), and the solid-phase fractions corresponding to the three temperatures are 0.55, 0.5, and 0.4, respectively. The distribution of entrainment air defects and oxide inclusion defects are shown in Figure 9. And

Figure 10 is a fitting diagram of the content of entrainment air and oxide inclusions contents as the time measured.

From the overall point of view of the casting, the internal entrainment air content is the highest when the die casting temperature is 580 °C, and the lowest when the die casting temperature is 590 °C. However, it can be seen from the corresponding nodes and the distribution of entrainment on the test bar that the entrainment air defects on the test bar are the least when the temperature is 570 °C. With the increase in die casting temperature, the content of oxidized slag in the casting has slightly increased, but the overall gap is not obvious. This is because the higher the temperature is, the faster the oxidation reaction occurs. In conclusion, 570 °C was selected as the best semi-solid die casting temperature.

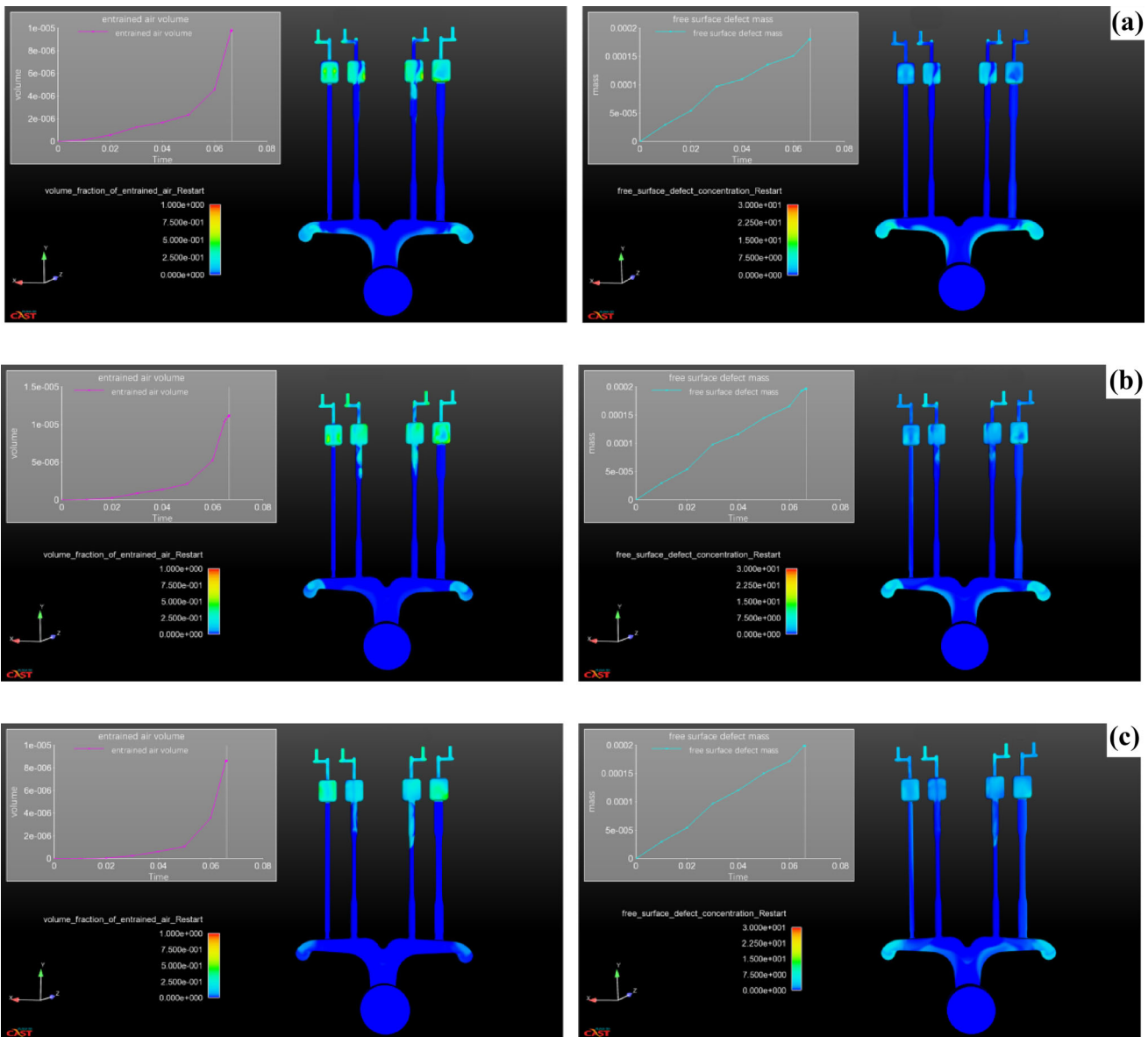


Figure 9. Defect distribution of entrainment air and oxide inclusions at different die casting temperatures (a) 570 °C, (b) 580 °C, and (c) 590 °C.

Structural Optimization Process and Simulation Analysis of Test Bar Overflow System

Detailed univariate analysis of injection rates and die casting temperature has been discussed in the foregoing, and the variation rules have been obtained. Detailed univariate analysis of injection speed and die casting temperature has been carried out in the foregoing, and their variation rules have been obtained. However, considering the mutual interference between the two parameters, two optimal process parameters (injection rates of 1 m/s, die casting temperature of 570 °C) have been used for simulation verification. The results are shown in Figure 11(a). It can be seen that the defects of the test bar are significantly reduced compared with the simulation results of other parameters. By changing the die casting process

parameters, the distribution of die casting defects is optimized to a certain extent, but the test bar still has certain defects, so it is necessary to optimize the structure of the test bar model. Firstly, the location of casting defects is determined by simulation analysis, so as to carry out reasonable design of overflow groove and venting channel. The setting of overflow grooves can collect the entrainment air and oxidation inclusions, and effectively reduce the defects generated inside the castings. The structure optimization process of the model and the corresponding simulation results after each optimization are shown in Figure 11.

Figure 11(a) is the initial test bar model. The simulation results show that there are obvious entrainment air defects at the upper ends of the two middle test bars, because the

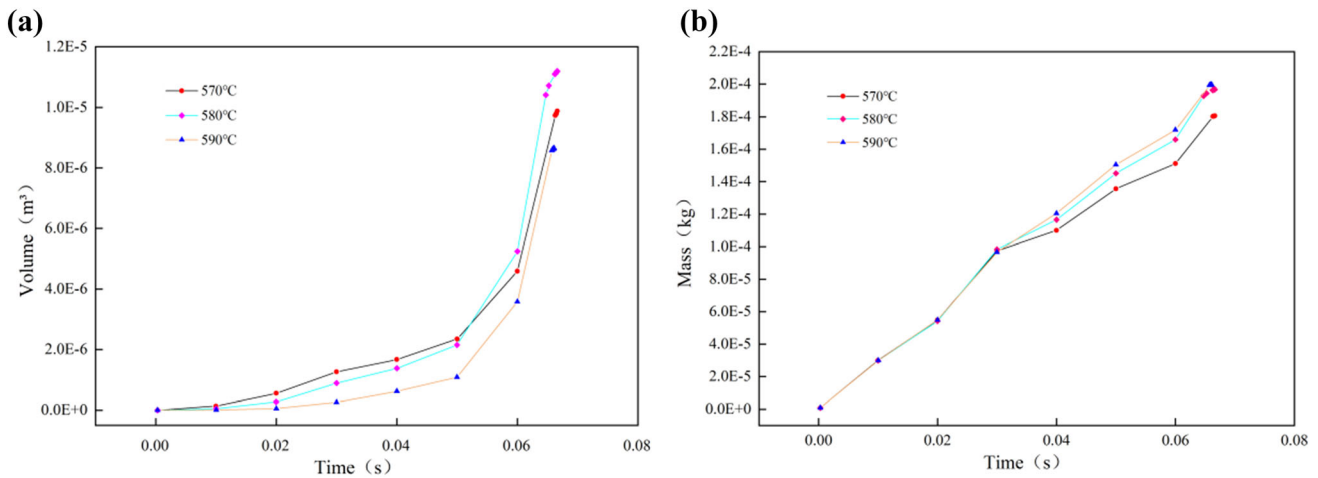


Figure 10. Defect contents versus filling time at different die casting temperatures (a) entrainment air, (b) oxide inclusions.

gas generated by the reflux of the molten metal cannot be discharged at the upper end of the test bars. Therefore, two overflow grooves are added at the upper end of the test bar where entrainment is easy to occur, as shown in Figure 11(b). The simulation results show that the entrainment air defect has been significantly improved, but there is still more entrainment. Meanwhile, the size of the model sprue was partially optimized, that was an extension of 10mm was added at the end of the sprue. The schematic diagram of the size optimization is shown in Figure 12. This optimization helped oxidation inclusions generated during mold filling to retain to reduce the defects of oxidation inclusions inside the casting. In order to increase the capacity of the overflow groove to collect gas and slag, the size was improved as shown in Figure 11(c). The simulation results after the increase in volume showed that the improvement effect was not obvious and there were still large entrainment air defects. Therefore, it was decided to add a venting system on this model, so that all the gas existing in the test bar can be exhausted through the venting channel, as shown in Figure 11(d). The simulation results show that the improvement effect of the entrainment gas defect is very obvious, and there is basically no entrainment air defect at the upper end of the test bar. Finally, the test bar model was further optimized and improved according to the experimental requirements, as shown in Figure 11(e). The exhaust duct connected to the overflow groove was thickened to make it easier to discharge the gas. In order to meet the experimental requirements, the thin sheet test bar on the left of the model was changed to a cylindrical test bar with the same size as the middle test bar. The corresponding simulation results show that the filling effect is good, and there is no entrainment air defect on the test bar. The cross-sectional size of the exhaust duct of the final model of the test bar is shown in Figure 13. The number of exhaust ducts connected to the overflow groove is the largest, so the cross-sectional size is the smallest, and the uppermost exhaust duct has the largest

cross-sectional size. This size design can better discharge gas inside the casting.

Analysis of Microstructure and Mechanical Properties of Test Bar

According to the die casting process parameters determined by the simulation results, the semi-solid die casting of the test bar was carried out. The main die casting process parameters are shown in Table 4. The die casting test bar is shown in Figure 14. By observing the casting surface, it can be found that the casting is completely filled with no obvious holes, cracks and other defects on the surface, which is basically consistent with the simulation results.

By observing its microstructure, it is found that the internal crystal grains are different from the coarse dendrites formed by ordinary liquid die casting. This kind of small and highly rounded spherical crystal grains can effectively reduce the solidification shrinkage and improve the feeding capacity of the metal, which can reduce or eliminate the tendency of shrinkage and improve mechanical properties. The OM picture is shown in Figure 15.

In order to have a deeper understanding of the microstructure, it will be characterized by the equal area circle diameter D and the shape factor F . The calculation formula is as follows:

$$D = \left(\frac{4A}{\pi} \right)^{\frac{1}{2}} \quad \text{Eqn. 3}$$

$$F = \frac{P^2}{4\pi A} \quad \text{Eqn. 4}$$

where A is the area of primary α -Al crystal grains, P is the perimeter of primary α -Al crystal grains.

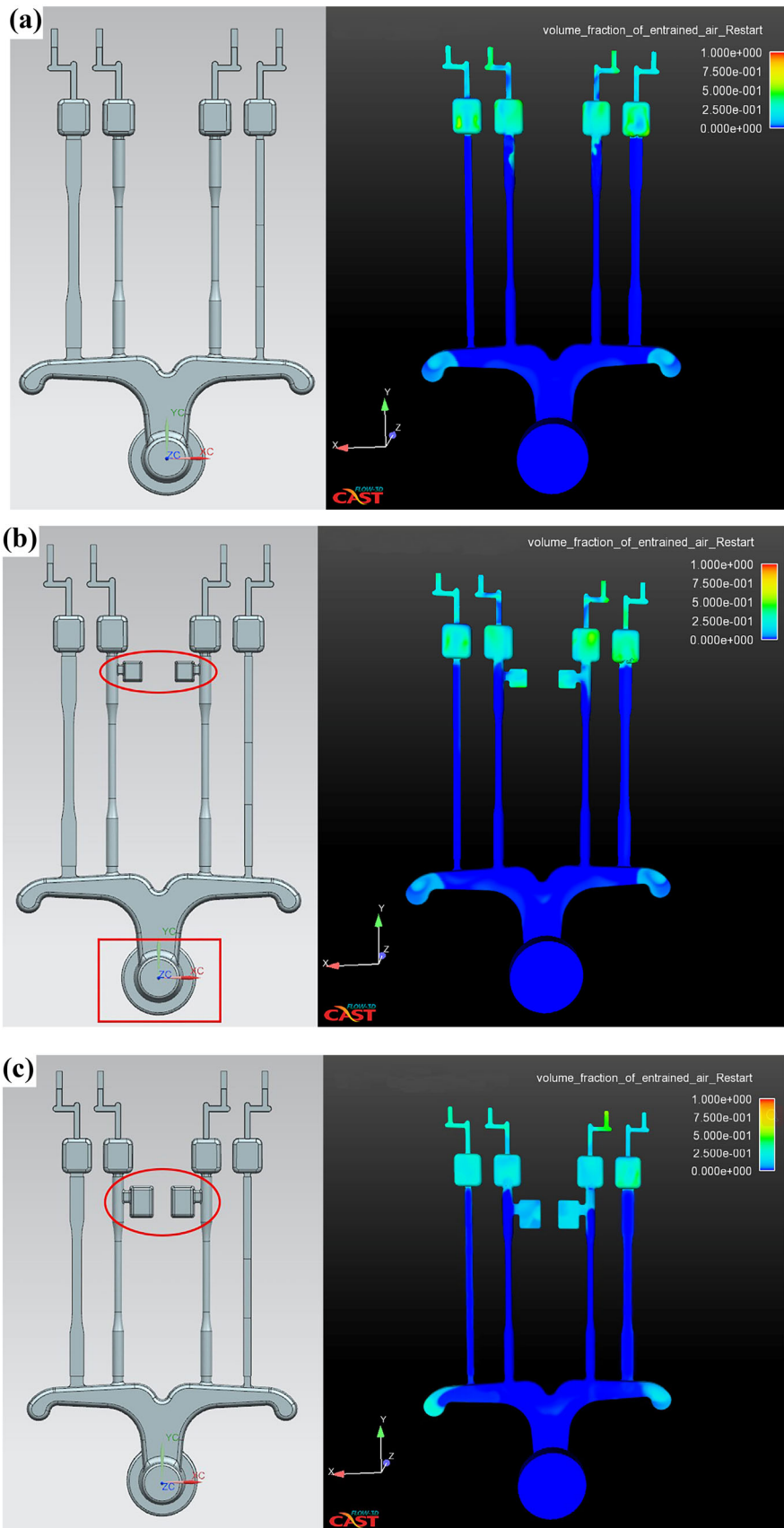


Figure 11. The structure optimization process and simulation results of the test bar model, (a) Initial model; (b) add overflow grooves; (c) optimize size of the overflow grooves; (d) add venting channel; e improve venting channel.

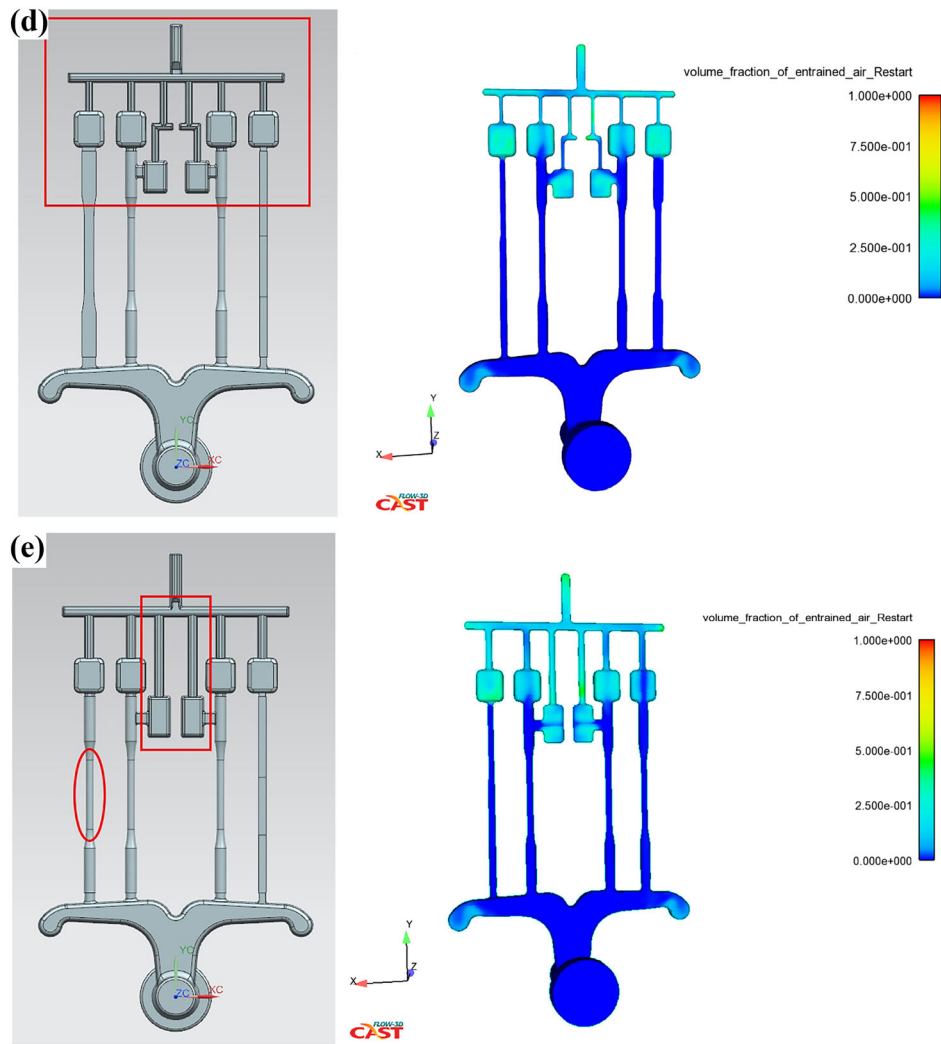


Figure 11. continued

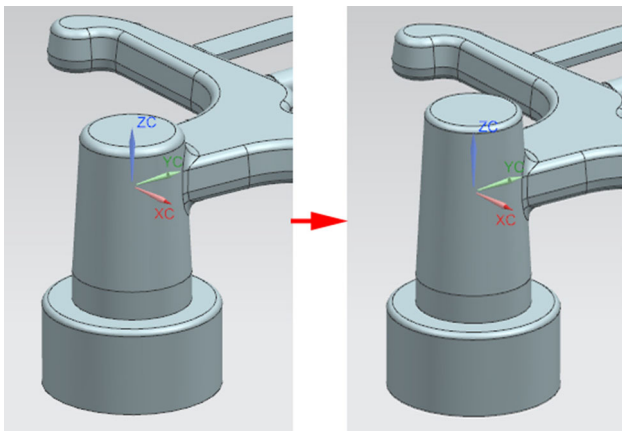


Figure 12. Optimization of sprue size.

The equal area circle diameter D can be used to more accurately characterize the crystal grains size, and the shape factor F can indicate the degree of crystal grain roundness. The closer the F value is to 1, the higher the roundness of the crystal grains are. The grain size is

calculated by the image analysis software Image-Pro-Plus 6.0. Each sample takes three different positions of the microstructure photographs for processing calculations to reduce errors. The average value of the three was taken as the final result. Through calculation, the average size of the α -Al grains inside the test bar is $28.27 \mu\text{m}$. The size distribution of the grains is shown in Figure 16 and is mainly distributed between 15 and $40 \mu\text{m}$. The average shape factor is 0.86, and the roundness of crystal grains is relatively high, which is a better semi-solid structure.

Scanning electron microscopy was used to observe the microstructure of the semi-solid and T6 heat-treated specimens, respectively. As shown in Figure 17, it can be found that in the semi-solid structure, the Al-Si eutectic phase in needle-like and fibrous forms, the irregularly-shaped white Al_2Cu phase and the second phases such as $\text{Al}_5\text{Cu}_2\text{Mg}_8\text{Si}_6$ are more evenly distributed around the α -Al matrix. After T6 heat treatment, eutectic silicon is gradually broken and spheroidized, changing from needlelike and fibrous to fine round particles evenly distributed around the matrix. And

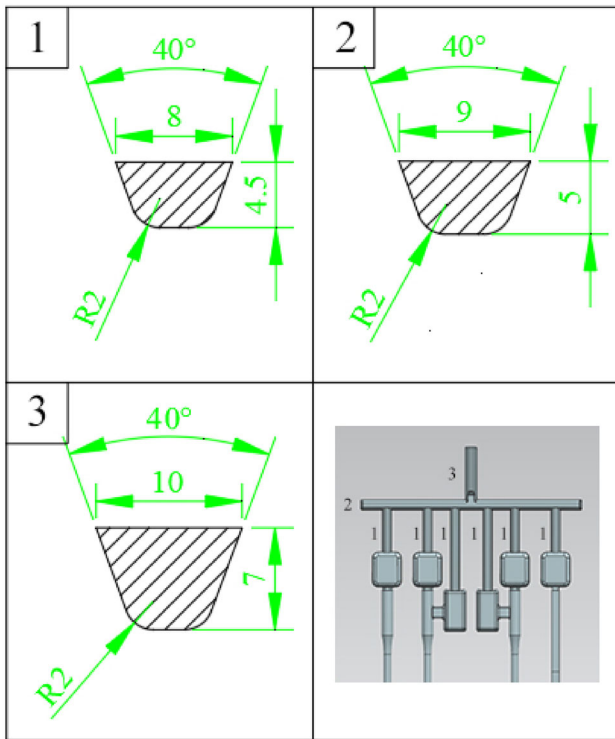


Figure 13. Size of venting channel.

Table 4. Main Die Casting Process Parameters

Parameters	Values
Pouring temperature	570 °C
Injection rates	1 m/s
Initial mold temperature	260 °C
Pressurization	100 MPa

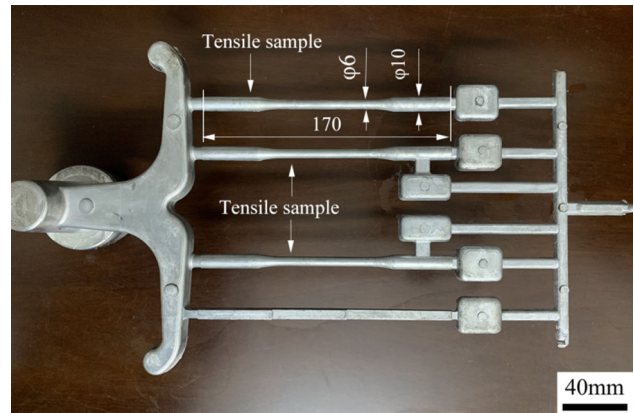


Figure 14. die casting test bar.

the other second phases have also been refined to a certain extent. In order to further determine the phases formed in the alloy, energy spectrum analysis was performed on the microstructure in both states. As shown in Figure 18. The transformation of the morphology and distribution of the strengthened phase in the alloy plays a crucial role in the improvement of mechanical properties.

The mechanical properties of the test bar were tested by tensile test. The tensile stress–strain curve of the test bar in the semi-solid and the T6 heat treatment state are shown in Figure 19. The tensile strength and yield strength of the semi-solid alloy are 269 MPa and 130 MPa, respectively, and the elongation is 7.3%. The test bar was strengthened by T6 heat treatment. The specific process parameters are as follows: solution temperature of 470 °C, time of 4h, aging temperature of 170 °C, aging time of 12 hours. After heat treatment, the tensile strength and yield strength can reach to 395 MPa and 345 MPa, the elongation is slightly reduced to 6.2%, and the tensile strength is increased by 47% compared with the semi-solid alloy. The reason for the decrease in elongation is that Al, Si, Cu and other elements in eutectic structure are continuously dissolved

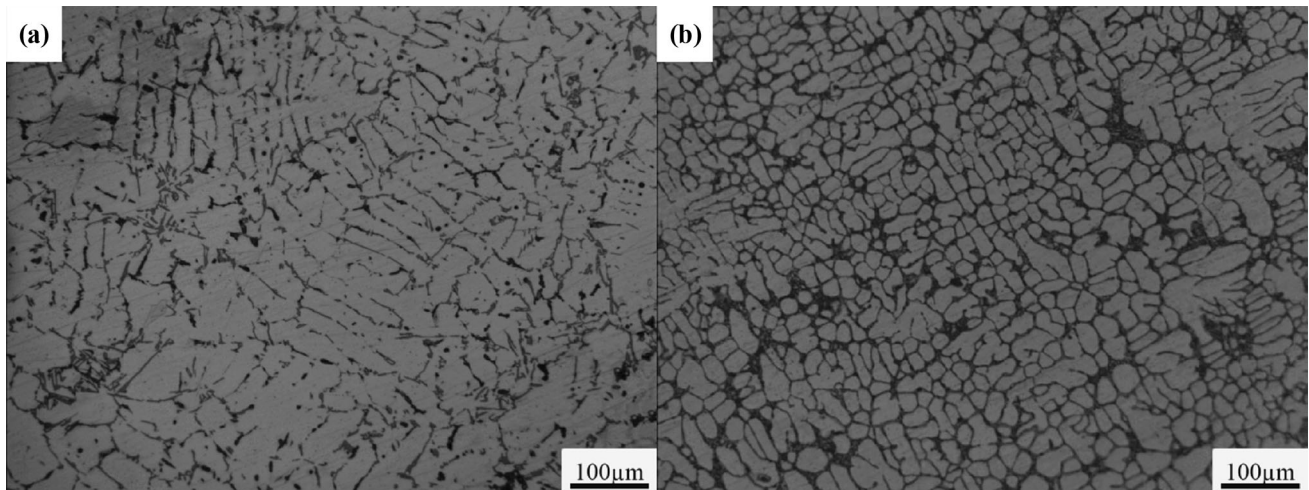


Figure 15. Die casting test bar OM picture (a) permanent mold casting, (b) semi-solid casting

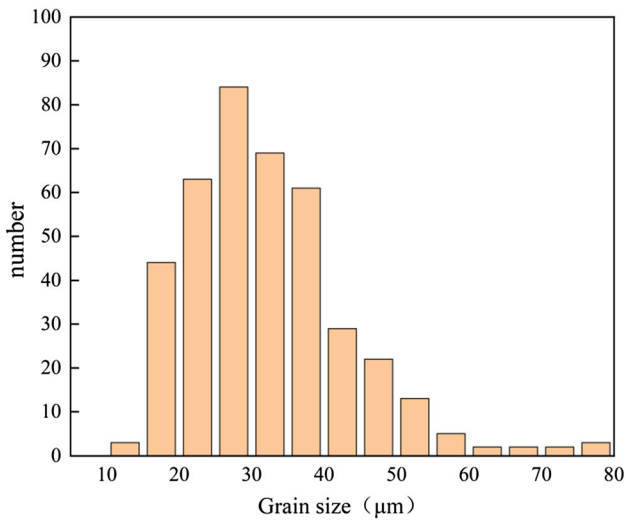


Figure 16. Grain size distribution map.

into the matrix and the second phase is continuously precipitated. As a result, the grain boundary between the matrix and the second phase becomes discontinuous, while the crack sources increase continuously during tensile. The

comparison of strength and elongation under the two conditions is shown in Figure 20.

The fracture of the test bar after stretching was observed and analyzed. The photographs taken by SEM are shown in Figure 21. It can be seen that at the fracture of semi-solid test bar, high stress leads to the plastic deformation of some grains and form tear ridge. And there are a few cleavage planes and river patterns. The fracture mode is quasi-cleavage fracture. After T6 heat treatment, the number and distribution of tearing edges at the fracture are decreased obviously, and the number and distribution of cleavage planes are increased, which results in the decrease in plasticity of the alloy.

Conclusion

1. Through numerical simulation analysis, it is found that with the increase in injection rate, entrainment air defect in casting gradually increases, while oxide inclusion defects gradually decrease. With the increase in die casting

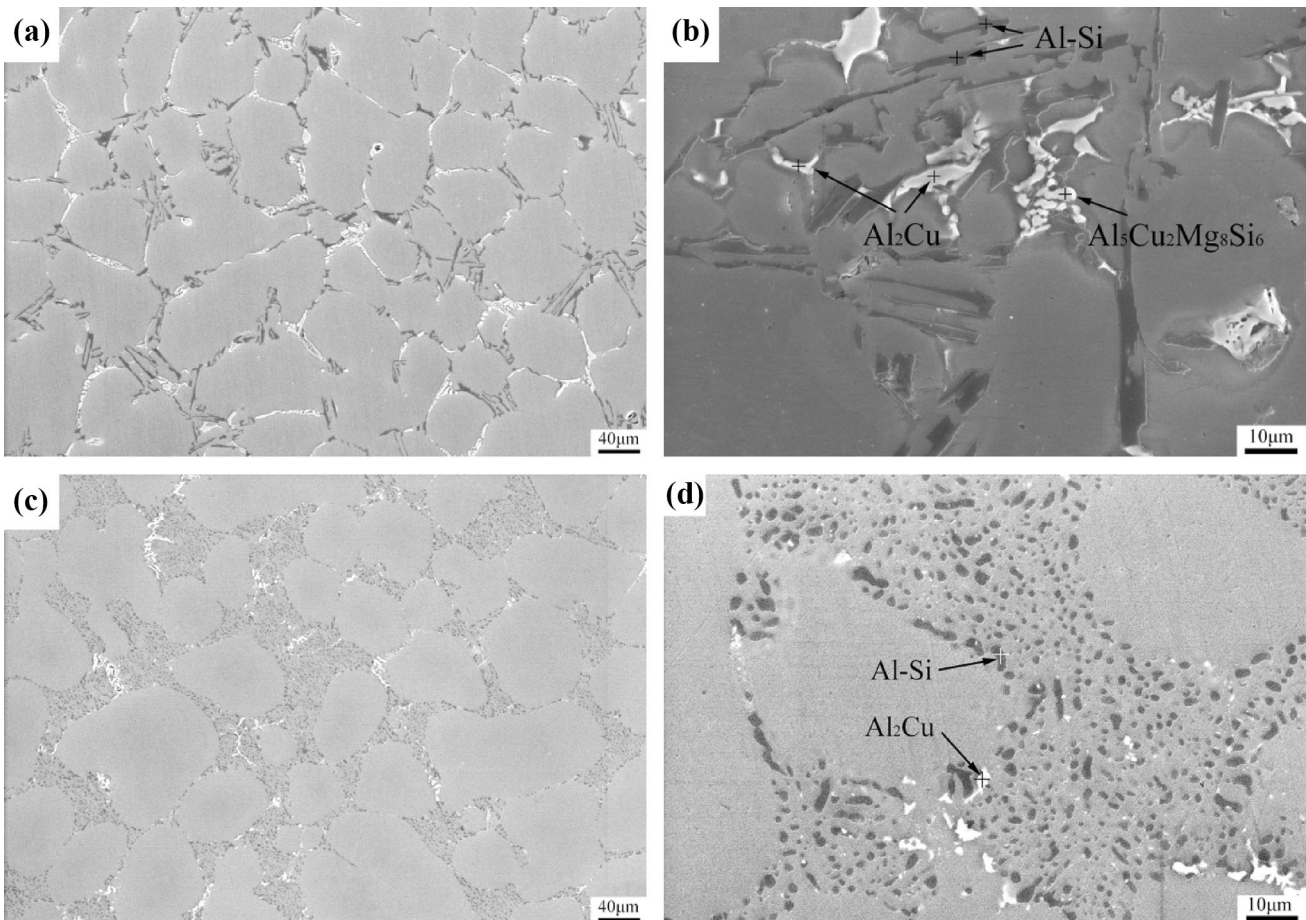


Figure 17. SEM images of the alloy (a, b) semi-solid and partial amplification, (c, d) T6 state and partial amplification.

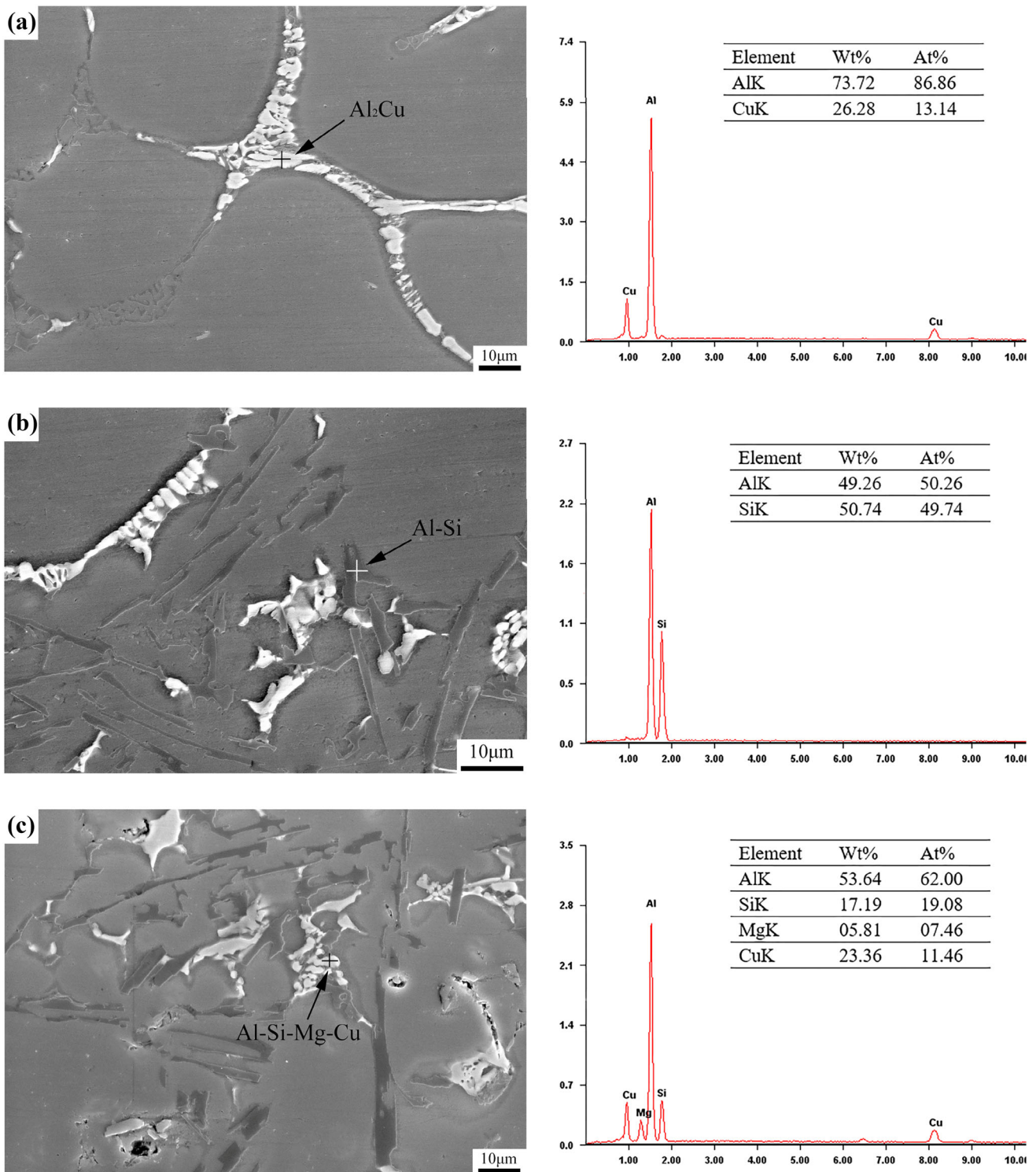


Figure 18. Energy spectrum analysis of microstructure in semi-solid state and T6 state (a–d) semisolid, (e) T6 state.

temperature, the entrainment air defect climbs up and then declines, while the change of oxide inclusion defects is not obvious. The optimal process parameters are injection rate of 1 m/s and die casting temperature of 570 °C.

2. Based on the simulation results, a series of structural optimizations were carried out on the

gating system of the model to eliminate internal defects. The optimization includes the design of the overflow groove at the entrainment air defect part of the upper end of the test bar, the extension of the straight sprue and the addition of the exhaust channel.

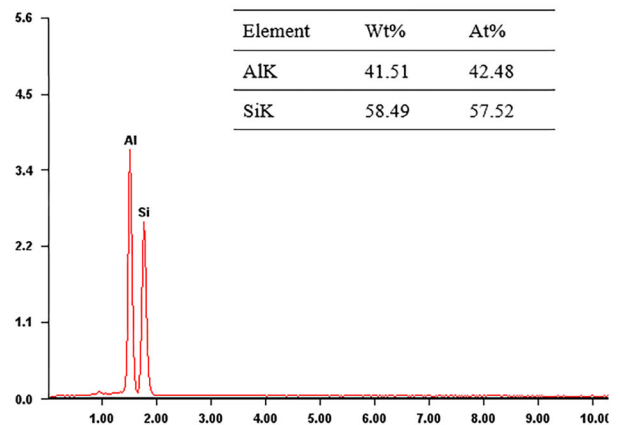
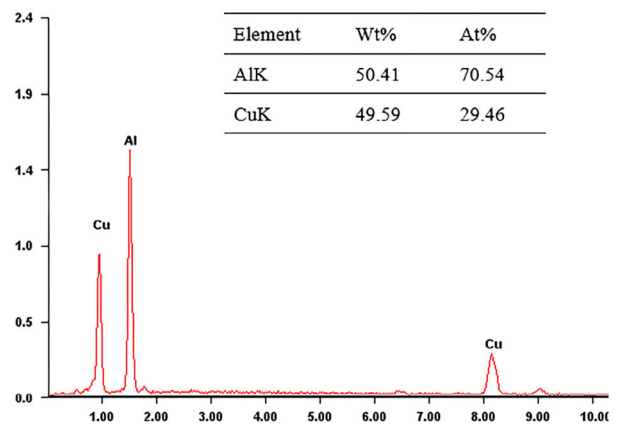
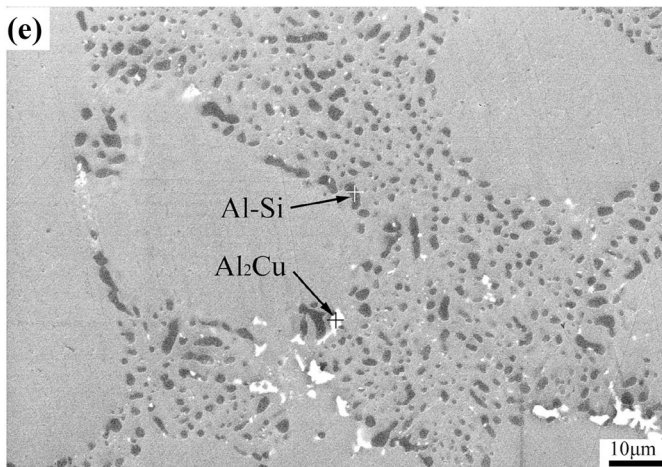
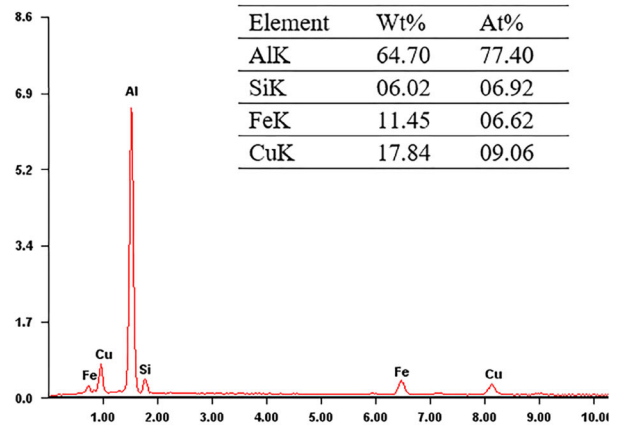
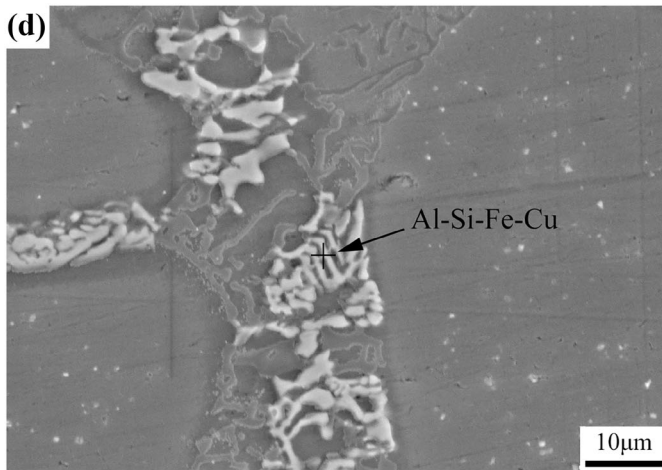


Figure 18. continued

3. The observation of the microstructure of the test bar showed that the internal microstructure grains were fine and round, with an average grain size of 28.27 µm and an average shape factor of 0.86, which was an excellent semi-solid microstructure. After heat treatment, the Al-Si eutectic phase in the alloy changes from the original

needle-like and fibrous shape to the fine spherical dispersed distribution, which significantly improves the mechanical properties of the alloy.

4. The mechanical properties of the castings were improved obviously by semi-solid forming process, with tensile strength of 269 MPa and elongation of 7.3%. After T6 heat treatment, the

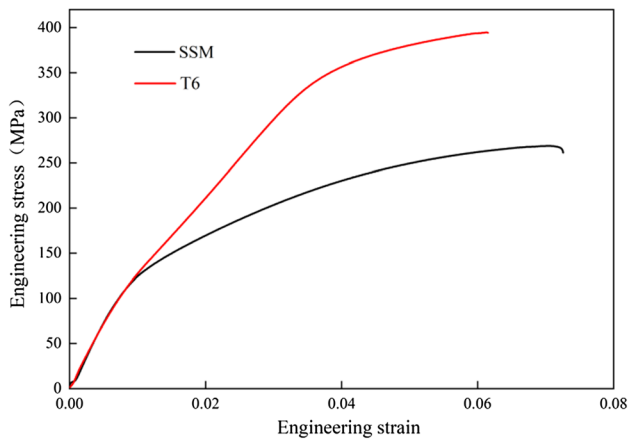


Figure 19. Tensile stress-strain curve in semi-solid and T6 state.

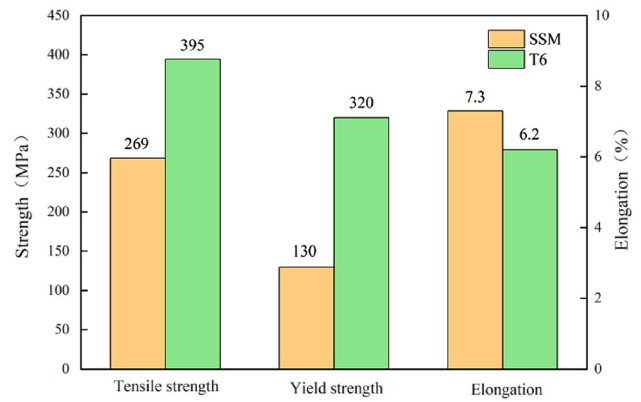


Figure 20. Strength and elongation of semi-solid state and T6 state.

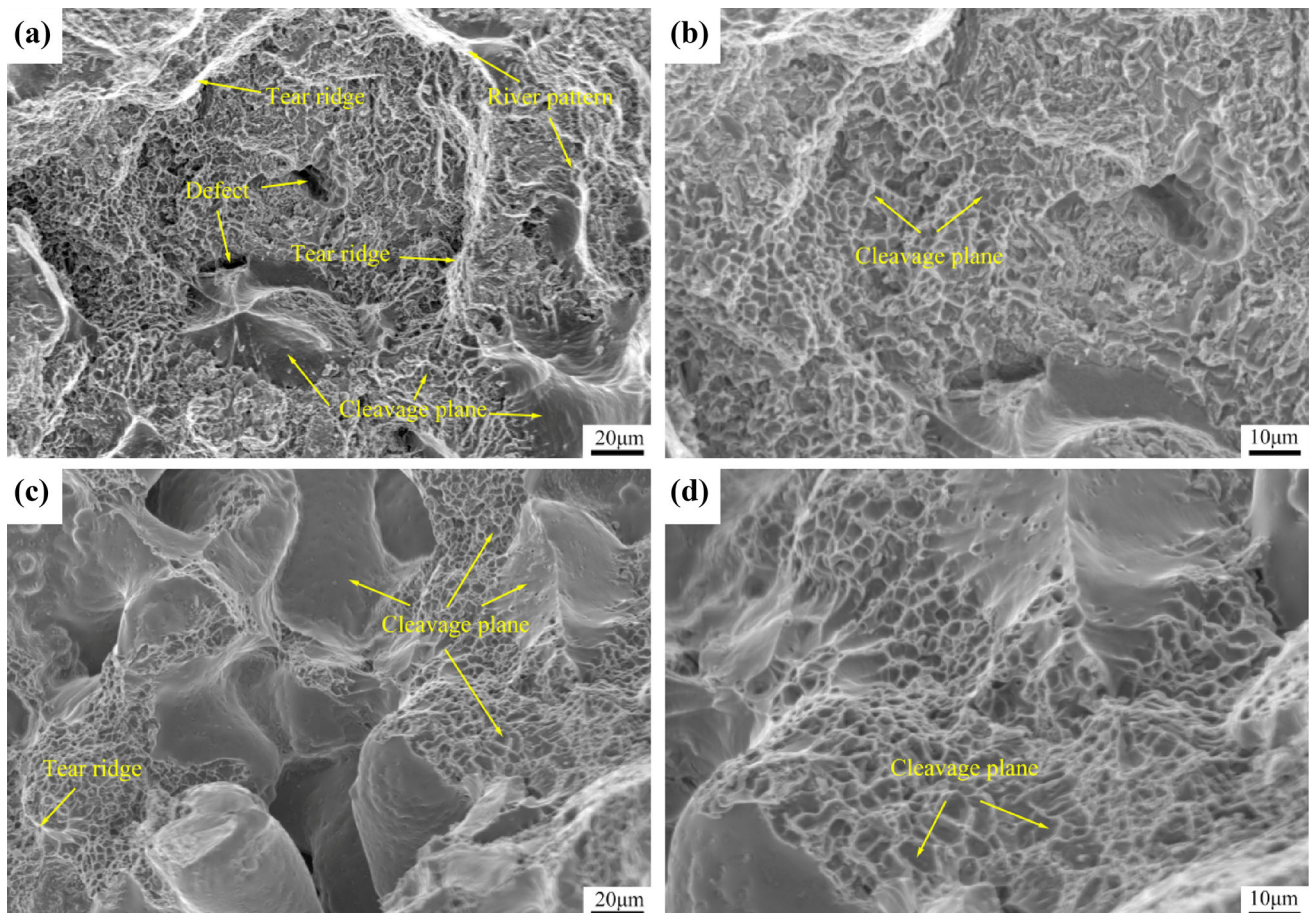


Figure 21. Tensile fracture morphology of alloy (a, b) semi-solid and partial amplification, (c, d) T6 state and partial amplification.

tensile strength of the test bar reaches to 395 MPa, 47% higher than that of the semi-solid state, but the plasticity is slightly reduced, with the elongation of 6.2%.

Acknowledgements

The authors would like to acknowledge the financial support from Innovation Talent Program in Sciences and Technologies for Young and Middle-aged Scientists of Shenyang (RC200414), Liaoning BaiQianWan Talents Program, Scientific research fund project of Liaoning Provincial Department of Education (LJGD2020008), Liaoning Revitalization Talents Program (XLYC1907007), High Level Innovation Team of Liaoning Province (XLYC1908006), Youth Project of Liaoning Education Department (Nos. LQGD2019002 and LJGD2019004), Department of Science and Technology of Liaoning Province (Grant Number 2019-ZD-0210).

REFERENCES

1. A.R. Adamane, L. Arnberg, E. Fiorese et al., Influence of injection parameters on the porosity and tensile properties of high-pressure die cast Al-Si alloys: a review[J]. *Int. J. Metalcast.* **9**(1), 43–53 (2015)
2. I. Duman, S. Jozi, D. Baji et al., Optimization of Semi-solid high-pressure die casting process by computer simulation, taguchi method and grey relational analysis[J]. *Int. J. Metalcast.* **15**(1), 1–11 (2020)
3. Y. Wang, S. Zhao, C. Zhang, Grain refinement of aluminum alloy bar by a modified RAP process for semi-solid Forming[J]. *Mater. Trans.* **58**(2), 176–181 (2017)
4. Kumai, Shinji, Prapasajchavet, et al., Microstructure Analysis of Al-5.5at%Mg Alloy Semi-solid Slurry by Weck's Reagent[J]. *Int. J. Metalcast.: Lead. Trans. Res. Technol. Global Metalcast.* **11**(1):123-130 (2017)
5. Z. Zhong, X. Zuo, X. Dong, et al., Progress in semi-solid forming technology for high strength aluminum alloy[J]. *Mater. Rev.* **27**(19):122-124+134 (2013)
6. L. Chen, Y. Zhao, F. Yan et al., Statistical investigations of serpentine channel pouring process parameters on semi-solid ZL101 aluminum alloy slurry using response surface methodology[J]. *J. Alloy. Compd.* **725**(25), 673–683 (2017)
7. S. Nourouzi, H. Baseri, A. Kolahdooz et al., Optimization of semi-solid metal processing of A356 aluminum alloy[J]. *J. Mech. Sci. Technol.* **27**(12), 3869–3874 (2013)
8. I. Dumani, S. Jozi, D. Baji et al., Optimization of semi-solid high-pressure die casting process by computer simulation, taguchi method and grey relational analysis[J]. *Int. J. Metalcast.* **15**, 108–118 (2021)
9. M.Y. Hu, J.J. Cai, W.L. Sun et al., DieCasting simulation and process optimization of An A356 aluminum alloy polishing plate[J]. *Int. J. Metalcast.* **10**(3), 315–321 (2016)
10. G. Li, H.X. Lu, X.G. Hu et al., Numerical simulation of slurry making process of 7075 aluminum alloy under electromagnetic field in rheocasting process[J]. *Solid State Phenom.* **285**, 373–379 (2019)
11. D. Vanluu, Numerical simulation on A356 aluminum alloy semi-solid slurry preparation with electromagnetic stirring[J]. *J. Mech. Eng.* **48**(14), 50–57 (2012)
12. S.Y. Ren, F. Wang, J.Y. Sun et al., Gating system design based on numerical simulation and production experiment verification of aluminum alloy bracket fabricated by semi-solid rheo-die casting process[J]. *Int. J. Metalcast.* **7**, 1–16 (2021)
13. B.C. Bhunia, Studies on die filling of A356 Al alloy and development of a steering knuckle component using rheo pressure die casting system[J]. *J. Mater. Process. Technol.* **271**, 293–311 (2019)
14. C.G. Kang, P.K. Seo, S.S. Kang, The effect of injection velocity on liquid segregation and mechanical properties in arm part fabricated by semi-solid die casting process [J]. *J. Mater. Process. Technol.* **176**(1–3), 32–40 (2006)
15. M. Perez, Computer simulation of the microstructure and rheology of semi-solid alloys under shear [J]. *Acta Mater* **48**, 3773–3782 (2000)
16. L. Kerrison, E.R. Galea, N. Hoffmann et al., A comparison of a FLOW3D based fire field model with experimental room fire data[J]. *Fire Saf. J.* **23**(4), 387–411 (1994)
17. C.W. Hirt, B.D. Nichols, Volume of fluid (VOF) method for the dynamics of free boundary. *J. Comput. Phys.* **39**(1), 201–225 (1981)
18. I. P. Jones, J. R. Kightley, C. P. Thompso, et al., FLOW-3D: A computer code for the prediction of laminar and turbulent flow, and heat transfer: release 1[M]. UKAEA Atomic Energy Research Establishment, (1985)
19. X.M. Wang, D.M. Zhang, Q.L. Zhang et al., Pipeline self-flowing transportation property of paste based on FLOW-3D software in deep mine[J]. *J. Central South Univ. (Sci. Technol.)* **42**(7), 2102–2108 (2011)
20. W. Lv, Z.Y. Yao, D.L. Zhang et al., Numerical simulation and analysis of 3-D internal flow field in mechanical turbulent coal pulverizer[J]. *Appl. Mech. Mater.* **170–173**, 3300–3303 (2012)
21. M.A. Hongyan, J. Yang, Study on refining and degassing during aluminum alloy smelting process[J]. *Metal Mater. Metall. Eng.* **46**(03), 34–38 (2018)
22. G. Fu, W. Yan, H. Chen et al., Influence of purification ways on the materials constant of 1235 aluminum alloy during Hot deformation[J]. *Spec. Cast. Nonferrous Alloys* **29**(07), 604–608 (2009)
23. J. Colbert, D. Bouchard, A heat transfer model for the production of semi-solid billets with the SEED process[J]. *Mater. Sci. Forum* **519**, 1525–1532 (2006)

24. P. Côté, M.E. Larouche et al., New developments with the SEED technology[J]. *Solid State Phenom.* **192**(3), 373–378 (2012)
25. C.G. Kang, J.W. Bae, Numerical simulation of mold filling and deformation behavior in rheology forming process[J]. *Int. J. Mech. Sci.* **50**(5), 944–955 (2008)

Publisher's Note Springer Nature remains neutral with regard to jurisdictional claims in published maps and institutional affiliations.